JTTEE5 13:93-107
DOI: 10.1361/10599630418077
1059-9630/$19.00 © ASM International

Sliding Wear Evaluation of Hot Isostatically Pressed Thermal Spray Cermet Coatings

V. Stoica, R. Ahmed, M. Golshan, and S. Tobe

(Submitted 21 August 2002; in revised form 10 December 2002)

The principal aim of this study was to compare the sliding wear performance of as-sprayed and Hot Isostatically Pressed (HIPed) thermal spray cermet (WC-12Co) coatings. Results indicate that HIPing technique can be successfully applied to post-treat thermal spray cermet coatings for improved sliding wear performance, not only in terms of coating wear, but also in terms of the total volume loss for test couples. WC-12Co coatings sprayed by a HVOF system were deposited on SUJ-2 bearing steel substrate and then encapsulated and HIPed at 850 °C for one hour. A high frequency reciprocating ball on plate rig was used to measure the sliding wear resistance of these coatings in dry conditions under steel and ceramic contact configurations at two different loads. Results are discussed in terms of coating microstructure, microhardness, fracture toughness and residual stress evaluations. Microstructural investigations indicate fundamental changes in grain morphology, whereas x-ray diffraction revealed beneficial transformations in phase composition of these coatings during the HIPing post treatment. The effects of these microstructural changes on the physical properties and wear resistance are discussed.

Keywords hot isostatic pressing, mechanical properties, microstructure, residual stress, sliding wear, thermal spray coatings, WC-Co, wear mechanisms

1. Introduction

Thermal spray coatings technology has evolved to be one of the preferred techniques for applying coatings of various metallic, ceramic, and polymer materials on a variety of substrates. The design of such surface engineered components thus caters to the economical, technological and environmental challenges faced by the industry. In wear-resistant applications, the coated layer provides the resistance to wear, while the substrate supports the impact to which the system (coating and substrate) is subjected. Various thermal spraying techniques can be used to achieve the best combination of coating and substrate properties for industrial applications. Nowadays, advances in thermal spraying make possible the replacement of bulk components in paper milling[1] or the replacement of chromium plating in aircraft manufacturing[2,3] or automotive industry.[4,5] Also the deposition of thermally sprayed coatings on critical parts in petroleum drilling[6] or on components in aero-applications such as fans and high-pressure compressors[7,8] were successful using detonation gun spraying (D-Gun), high velocity oxygen fuel (HVOF), and atmospheric plasma spraying (APS).

To bear the severe wear conditions in service life, a component should have, beside the high hardness, an acceptable level of fracture toughness. It is widely recognized that tungsten carbide-cobalt has the required combination of high hardness of tungsten carbide grains and the ductility of metal cobalt. Moreover it was reported that, among other carbides, tungsten carbide has the added ability to deform plastically without fracturing.[8] These special features offer an excellent combination of tribological properties for applications, which require resistance to sliding and abrasive wear.

Beside the powder characteristics, the process of spraying plays an important role in achieving good quality coatings for wear resistant applications. The low temperature and also the high velocity of the flame are the two main requirements for producing these coatings. A better understanding of all the parameters involved in the process, which alter the temperature and velocity of the flame are therefore needed. An ideal spraying system would be one that balances the thermal and kinetic energies and finds a compromise between them. Therefore an optimum temperature and velocity, first decreasing the degree of chemical reactions that occur in powder particles during deposition, and second decreasing the average dwell time to promote a mechanical bonding during coating formation, are needed. HVOF has proved to be one of the best techniques to deposit wear-resistant carbide cermet-type coatings. The high velocity (around 1500 m/s) of particles sprayed on the substrate compensates for the low powder temperature (around 2800 °C), resulting in hard dense coatings, with low residual stress (tensile or compressive). Moreover, HVOF-deposited coatings exhibit less phase transformations and lower porosity compared with other spraying techniques.

However, the combination of low temperature and high velocity has the disadvantage of relatively low fracture toughness due to poor bonding at the interfaces between the unmelted and semi-melted particles. Also, some phase transformations occur and the resulting products, which are generally brittle, decrease the wear resistance of the coating. Therefore, even for coatings

V. Stoica and **R. Ahmed,** Heriot Watt University, School of Engineering and Physical Sciences, Riccarton, Edinburgh, EH14 4AS, United Kingdom; **M. Golshan,** CLRC, Daresbury Laboratory, Warrington, Cheshire, WA4 4AD, United Kingdom; **S. Tobe,** Ashikaga Institute of Technology, 268 Ohmaecho, Ashikagashi, Tochigiken-326, Japan. Contact e-mail: R.Ahmed@hw.ac.uk.

which were produced by the last generation of HVOF systems, it can be beneficial to apply a post treatment to achieve the best results in applications requiring high wear resistance. Hot isostatic pressing (HIPing) has proved its value as a post treatment of thermal spray coatings in providing an attractive combination of material properties.[10-15] Although a limited number of studies are found in published literature, the authors reported significant improvements in the properties of APS coatings due to HIPing post-treatment. In general, the hardness and density of the coating increased while the porosity substantially decreased.[12-14] It was also reported that a change from lamellar to granular structure[10,11] and also metallurgical bonding at the splat/splat and coating/substrate interfaces[15] could occur during HIPing. The aim of the present investigation was thus to compare the sliding wear resistance of as sprayed and post treated WC-12 wt.% Co coatings, deposited by the HVOF process, using a reciprocating ball on plate machine. The changes experienced by the cermet coating are explained in terms of microstructure, hardness, fracture toughness, residual stresses, and sliding wear resistance.

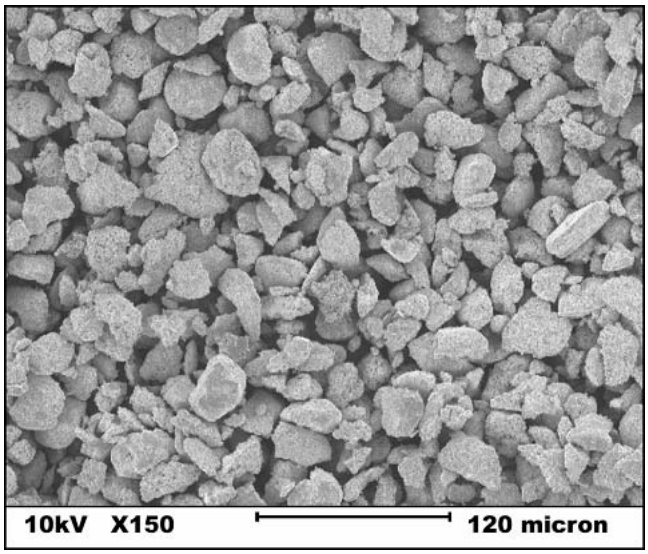

Fig. 1 Sintered and crushed WC-12Co powder

2. Experimental Procedure

2.1 Material Selection

The material selected for this evaluation was sintered and crushed WC-Co powder with 12 wt.% Co. The size distribution measured by optical microscopy ranged from 15-50 μm. The mean particle size was 30 μm. Figure 1 shows the scanning electron micrograph of the powder.

2.2 Coating Production and Post Treatment

Thermal spray coatings were produced by the HVOF process using a JP5000 system on SUJ-2 (AISI equivalent 52 100) bearing steel disks of 31 mm diameter and 8 mm thickness. Oxygen and kerosene were mixed in the combustion chamber, forming gases that accelerated the powder particles through the nozzle onto SUJ-2 steel substrate. The substrate was grit blasted and preheated prior to deposition. The HIPing treatment was carried out in argon environment at a fixed temperature and pressure of 850 °C and 150 MPa, respectively. The sprayed samples were encapsulated and heated at a rate of 50 °C/h until the desired temperature was reached, kept at 850 °C for 1 h after which they were cooled at a rate of 30 °C/h. Then, the encapsulations were removed and the coating surface ground and polished to achieve an average coating thickness of 200 μm.

2.3 Coating Characterization

X-ray diffraction (XRD) analysis was used to quantify the microstructural changes for both the as-sprayed and HIPed coatings. The diffraction patterns were obtained with a D500 diffractometer (Bruker AXS Limited, UK) operating at 40 keV and 20

Table 1 Ball Properties

Property	440C Steel	Si_3N_4
Diameter, mm	12.7	12.7
Density, kg/m^3	3165	7769
Weight, g	~3	~8
Average roughness R_a, μm	0.015	0.013
Hardness (HV0.1), kg/mm^2	820	1580

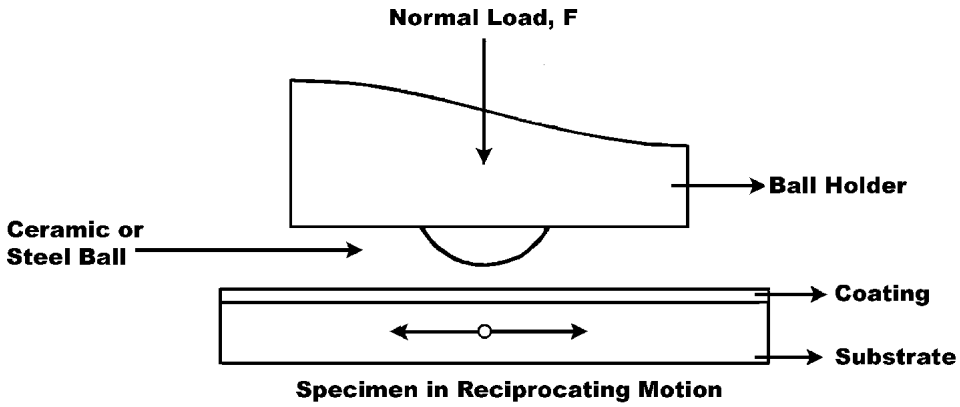

Fig. 2 High-frequency reciprocating ball on plate rig

mA. Cu K_α radiation was used, and the samples were run at 2θ from 10°-90° with a step size of 0.02° (2θ) and a time of 2 s/step.

Coating microstructure was evaluated by scanning electron microscopy using conventional imagining with secondary and backscattered electrons (SE and BSE). Microhardness evaluations were performed on the metallographic samples on coatings surface and its cross section. Each value presented (Sec. 3.2) was an average of thirty-six measurements performed at a load of 300 g (2.9 N), using a Vickers microhardness test machine. Care was taken to avoid the edge effect and also the influence that one indentation might have on a neighboring one. For the cross-section measurements, the samples were mounted in epoxy, and indentations were applied at three different depths in the polished coating cross section.

Fracture toughness and Young's modulus were also measured by the indentation method. Fracture toughness measurements were carried out on the coating surface using a load of 10 kg. The values of elastic modulus, obtained from the force indentation curve, were calculated out of the so called "elastic penetration modulus" from indentations performed on the coating

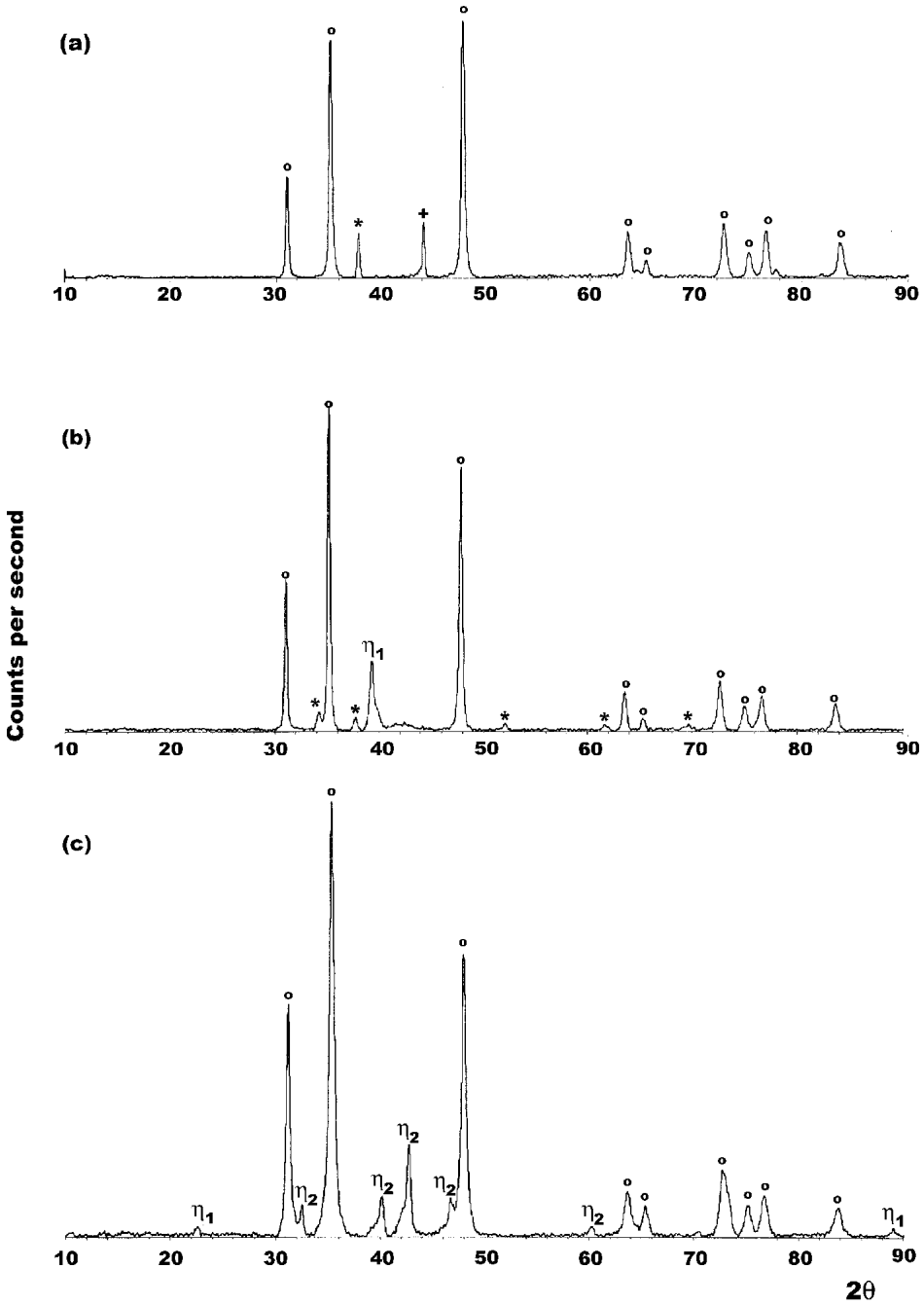

Fig. 3 XRD spectras of **(a)** powder, **(b)** as-sprayed HVOF, and **(c)** HIPed coatings. (o) = WC, (*) = W_2C, (^) = W, (+) = Co, $(\eta)_2 = Co_3W_3C$, $(\eta_2) = Co_6W_6C$

surface at 1000 mN and on the coating cross section using a test load of 500 mN. A complete description of the measurement procedures can be found in Buchmann et al.[16]

Measurements of the residual stress distribution within the as-sprayed and HIPed coatings were performed using x-ray synchrotron radiations. The $\sin^2\psi$ method was applied with three ψ angles between 7° and 9° at 25 keV and between 12° and 14° at 15 keV. The shift of the diffraction peak was recorded and the magnitude of the shift related to the magnitude of the residual stress through the slope of the $2\theta - \sin^2\psi$ plot. A similar approach was used to calculate the residual strain. The peak position was determined using the peak center of gravity.

2.4 Tribological Testing

Sliding wear tests were carried out using a reciprocating ball-on-plate apparatus, instrumented to measure the frictional force via a load cell (Fig. 2). Balls were commercial grade 440C steel and silicon nitride (Si_3N_4) ceramic, whose hardness and roughness values are listed in Table 1. The coated specimens were ground and polished to produce a surface roughness (R_a) of 0.04 μm. In the setup shown in Fig. 2, the upper ball bearing the normal load is stationary, while the coated disk has a sliding speed of 0.03 m/s at the center of the wear scar. Before each test, the coatings and balls were ultrasonically cleaned in acetone for 5 min to remove any contaminants and grease, dried in air, and weighed. The tests were performed under two normal loads (4 and 6 kg) in unlubricated contact conditions at ambient temperature and humidity. Corresponding to the load of 4 kg, the stresses at the beginning of the test were 0.85-0.87 GPa for the as-sprayed and HIPed coatings tested versus steel balls, and 0.98-1 GPa for the coatings sliding over ceramic balls, respectively. At 6 kg load, the contact pressure was 0.97-0.99 GPa for the as-sprayed and HIPed coatings tested versus steel balls, and 1.12-1.15 GPa for the tests involving ceramic balls. Each test was repeated two times to confirm the relative trends of various test couples, the results of which are shown later in Sec. 3.3.

The coating wear scars were examined using Zygo NewView (Lambda Photometrics Ltd, UK) 5000 interferometer, which provided the volume loss of the material for each wear scar. The volume loss of the ball was evaluated using an optical microscope, which allowed the precise measurement of the ball wear scar diameter. Moreover, using the diameter of the sphere segment removed during the test, the ball volume loss (V) was calculated as

$$V = \frac{\pi H^2}{3}(3R - H), \quad \text{(Eq 1)}$$

$$\text{where } H = R - \sqrt{R^2 - r^2}, \quad \text{(Eq 2)}$$

and R and r are the ball radius and ball-wear-scar radius, respectively. The surface morphology of the ball and coating wear scars and the wear debris were analyzed with SEM equipped with energy-dispersive x-ray (EDX).

3. Experimental Results and Analysis

3.1 Microstructural Identification

3.1.1 X-ray Diffraction Analysis. The XRD patterns of the spray powder, as-sprayed and HIPed coatings are presented in Fig. 3. The powder profile shows only tungsten carbide (WC) and cubic cobalt (Co) peaks. A small amount of secondary phase tungsten carbide (W_2C) is also present, probably produced during the sintering process of powder manufacturing. It is obvious from Fig. 3 that the coating deposition process led to the thermal decomposition of WC, since the x-ray profile of the as-sprayed coating indicates the occurrence of higher amounts of secondary phase tungsten carbide (W_2C) than the spray powder. Some η phases (Co_3W_3C) can also be observed from the profile. This was expected in view of the published literature,[17-21,23,25] explaining that the coatings deposited by the HVOF systems can undergo some degree of phase transformations (see reactions below). No metallic Co was observed in the coating after deposition, suggesting that part of metallic tungsten and carbon resulted after decomposition reactions diffused into the cobalt binder. Therefore, an amorphous or nanocrystalline binder phase was produced. This is consistent with other investigations where a small hump that indicates an amorphous or nanocrystalline phase was present in the profile at approximately $2\theta \simeq 42°$.[18-21,24,25] Part of carbon, which did not dissolve in the ma-

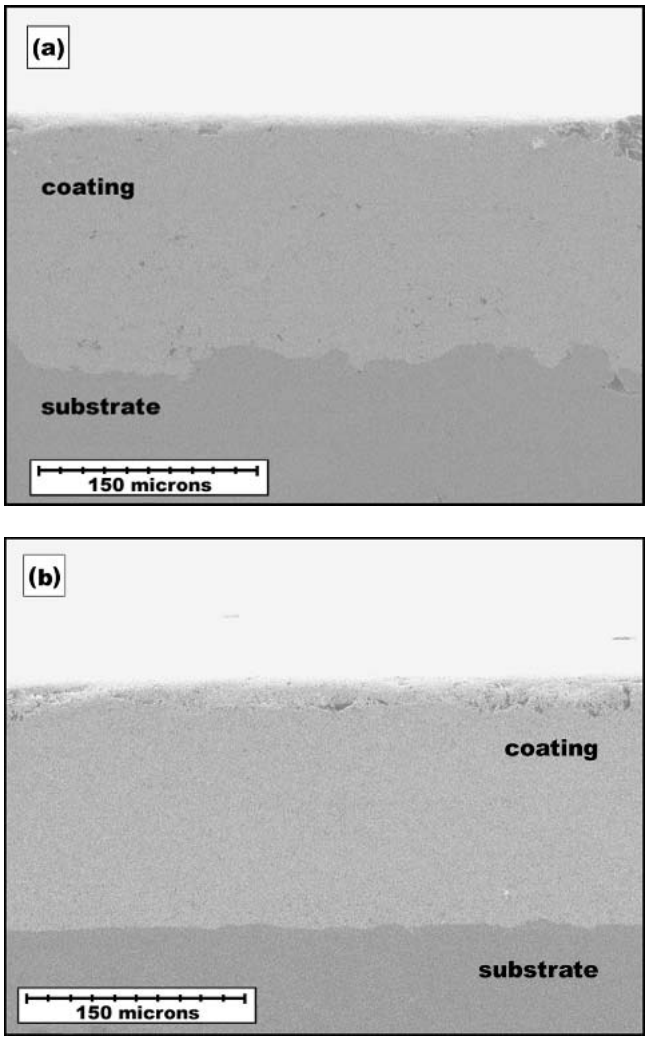

Fig. 4 SEM micrographs on cross-section of **(a)** as-sprayed and **(b)** HIPed coatings

trix, was eliminated by oxidation while tungsten was seen in the as-sprayed coating with possible reactions:

$$WC \rightarrow W_2C + C$$

$$W_2C \rightarrow 2W + C$$

$$2C + O_2 \rightarrow 2CO$$

After HIPing post treatment at 850 °C, the amorphous phases can not be seen in the HIPed coatings. Differential thermal analysis (DTA) carried out by Li et al.[24] on WC-Co HVOF deposited coatings revealed two exothermic reactions at 660 and 830 °C. The first was identified as the recrystallization reaction of the amorphous phase forming metallic cobalt, complex carbides and tungsten, and the second as the reaction of crystallized tungsten and cobalt with carbon to form additional complex carbides. The DTA analysis performed by Nerz et al.[23] also indicated a strong exothermic reaction at around 860 °C whose products were complex carbides (Co_6W_6C and Co_2W_4C) (see also Ref. 21, 22). In the present investigation, during HIPing at 850 °C, the recrystallization reaction more likely occurred, which is consistent with the studies by Li et al.,[24] i.e., during initial heating at a temperature above 650 °C to form cobalt, a large amount of cobalt-containing phases (Co_3W_3C and Co_6W_6C), and also tungsten. Moreover, it is believed that at the HIPing temperature of around 850 °C, the recrystallized cobalt reacted with secondary phase of tungsten carbide and probably with tungsten producing complex η phases, with possible reaction:

$$W_2C + W + 3Co \rightarrow Co_3W_3C$$

This reaction explains the elimination of secondary phase W_2C,[22] the absence of recrystallized Co and W and the formation of η phase in the HIPed coating. Slight increase in the

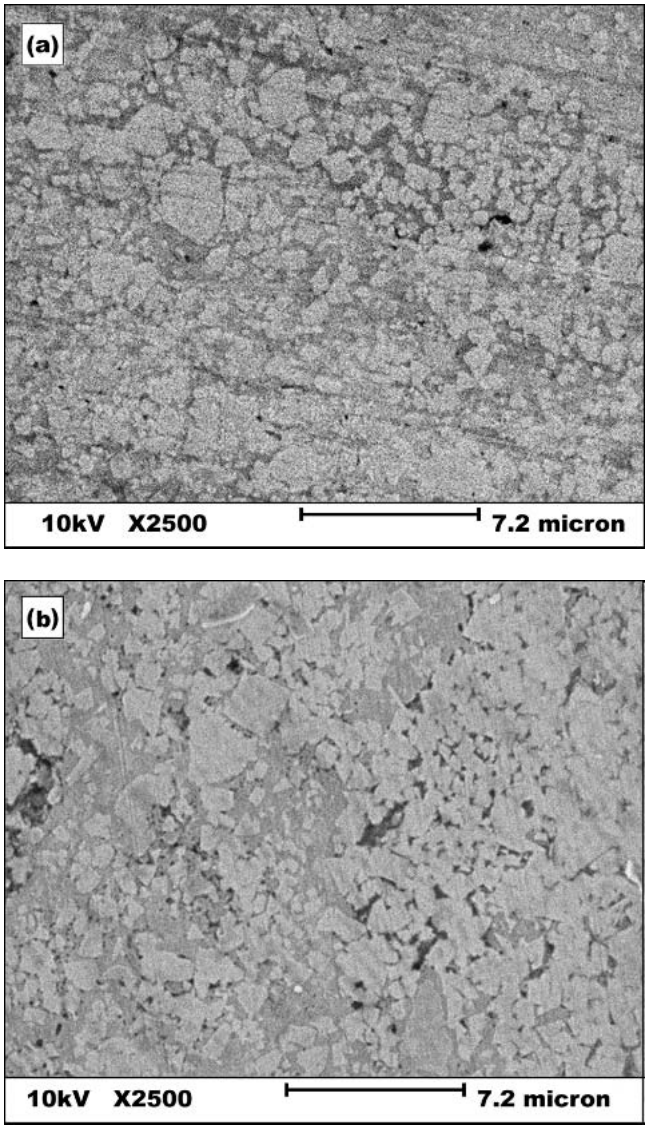

Fig. 5 High-magnification SEM micrographs on cross-section of **(a)** as-sprayed and **(b)** HIPed coatings

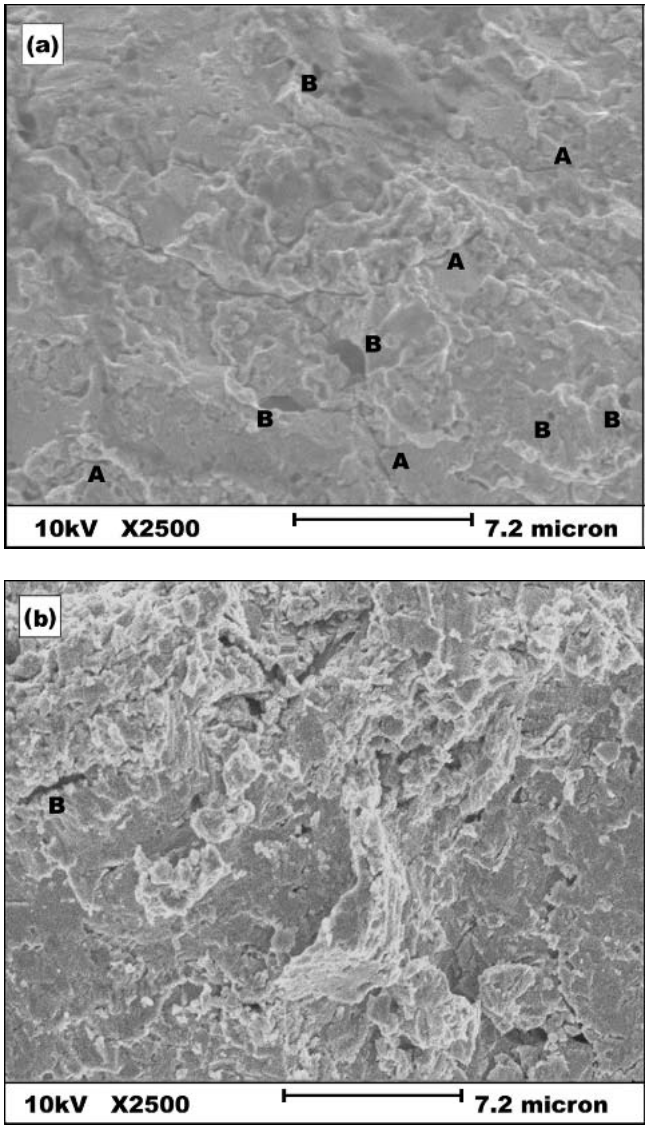

Fig. 6 SEM micrographs on cross-section of cryogenic fractured a **(a)** as-sprayed and **(b)** HIPed coating

amount of mono tungsten carbide and higher peaks of η phase than in the as-sprayed coating were also seen after HIPing. Furthermore, during HIPing, the Co_3W_3C transformed to Co_6W_6C whilst new peaks of Co_3W_3C occurred.

3.1.2 SEM Observations. In addition to the phase transformation investigation, the microstructure of both the as-sprayed and HIPed coatings was evaluated using a scanning electron microscope. Low-magnification micrographs are presented in Fig. 4. The first sign of the influence of HIPing post treatment on coatings microstructure can be clearly observed at the coating/substrate interface. The result of the grit-blasting process prior to coating deposition was the increased roughness of the substrate (Fig. 4a), thus mechanically interlocking the splats. On the other hand, under the pressure and temperature of the HIPing process, the steel substrate is pressed until the asperities, which form the roughness of the steel surface, are plastically deformed. Therefore a smooth coating substrate interface was observed after the HIPing post treatment.

Higher magnification SEM images reveal the difference in tungsten carbide grain morphology between the as-sprayed and HIPed coatings (Fig. 5). Image analysis was carried out on both types of coating. It was concluded that there is no significant difference in the carbide grain size, but the as-sprayed coating shows a rather homogeneous distribution of the grains over the binder phase. The diffusion mechanisms during HIPing led to the formation of prismatic interfaces of the grains. This is explained by the solubility of the tungsten carbide in cobalt, which produces a decrease in the activation energy for atomic movement. Close-packed boundaries are produced, and therefore agglomerates of tungsten carbide grains are seen along the coating. However, the formation of these homogeneous aggregates brings about an increase in the size of the binder areas, which contain only few scattered carbide grains.

For the sake of limited space the authors did not include high magnification micrographs of the interface between the coating and the substrate. However a close examination of these micrographs reveals a phenomenon that occurs at the interface during the post treatment. This is the precipitation of needle-shaped WC grains during the HIPing process. However, at this stage it could not be confirmed if any diffusion of steel in the coating material or visa-versa took place.

To have a qualitative evaluation of the degree of coating porosity by means of image analysis, and to avoid any confusion about the measured porosity being the true porosity or that which arose from the metallographical preparation, i.e., material pull-out [e.g., Ref. 27-29], the coatings were immersed in liquid nitrogen for three hours and then fractured. The as-sprayed coatings (Fig. 6a) exhibit cracks (A) and pores (B), whose sizes range from 0.5 μm to around 2 μm. During the HIPing process, it is believed that the short cracks and the pores whose size is around 0.5 μm collapses under pressure (Fig. 6b). The long cracks were fragmented while bigger pores were flattened having now the aspect of small cracks. Worth mentioning here is also the fact that the surface of the fractured HIPed coating was much rougher than that of the as-sprayed coating. This suggests that the cracks find their way through the coating more difficult, therefore consuming more energy to propagate in HIPed coating.

Table 2 Averaged Microhardness Data

Distance From Interface	HV0.3	
	As-Sprayed	HIPed
50 μm	1348.8 (±104.16)	1493 (±70.97)
100 μm	1395.9 (±111.94)(a)	1578.8 (±73.06)
150 μm	1384.4 (±97.89)(a)	1603.5 (±119.49)
Surface	1252.7 (±106.56)	1670 (±153.89)

(a) The values were measured at 90 and 120 μm, respectively.

3.2 Mechanical Testing

3.2.1 Microhardness. The microhardness values for both the as-sprayed and HIPed coatings are listed in Table 2. The

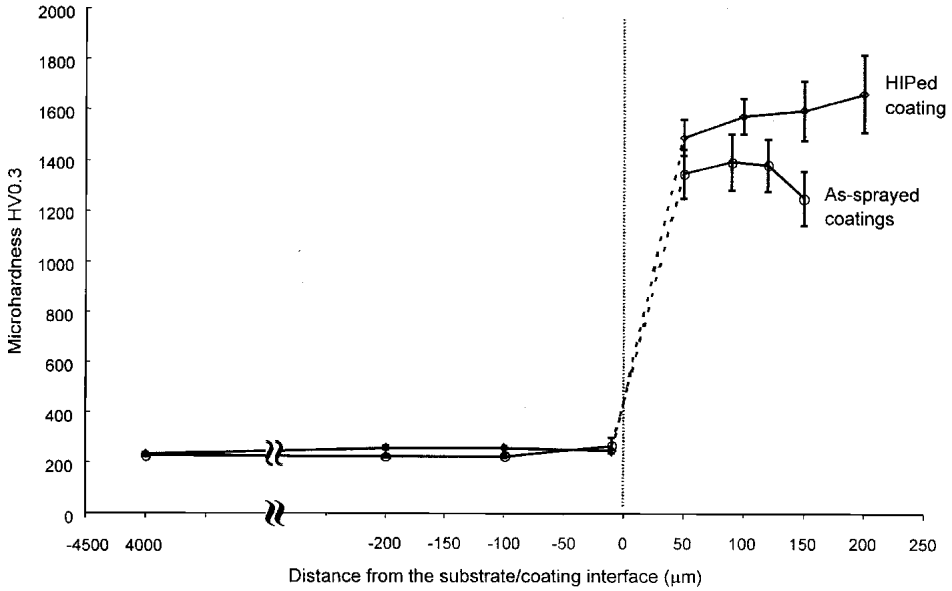

Fig. 7 Variation of microhardness with the distance from the substrate/coating interface: **(a)** as-sprayed and **(b)** HIPed coating

microhardness was measured on the surface and on the coating cross section at three different depths from the coating-substrate interface at a load of 300 g (2.9 N). Variation of hardness with the distance from the coating substrate interface is shown in Fig. 7.

These results indicate an increase in coating microhardness after the HIPing post treatment, which ranges from ~10% at 50 μm from the interface to ~30% on the surface of the coatings. This increase is related to the phase transformations that occurred during the post-treatment. Although the harder secondary phase W_2C was eliminated during the HIPing post-treatment, the recrystallization reactions replaced the amorphous phase with the harder η phases. Thus, the simultaneous effect of the binder hardening and the increase in the amount of mono tungsten carbide led to an overall increase in the hardness of the HIPed coatings. Moreover, the described microstructure of the treated coating with tungsten carbide agglomerates helps bearing higher loads than the as-sprayed coating. As shown in Fig. 7, throughout the depth of the coatings, the hardness of the HIPed coating is higher than the as-sprayed coating. This variation of hardness with coating depth also suggest that the region of the coating more affected by the high temperature and pressure of the post-treatment, which is obviously near the coating surface, exhibit higher hardness. Therefore, the hardness improvement is greater as the distance from the coating/substrate interface increases.

3.2.2 Fracture Toughness The indentation method of fracture toughness measurement was used using several loads. However, even with the highest load (25 kg) and repeating the measurements five times, the crack length on the HIPed coatings could not meet the criteria $c > 2a$, required for the determination of numerical value of fracture toughness.[26] In this criterion, c represents the crack length and $2a$ is the indentation diagonal. Therefore a quantitative analysis of the fracture toughness could not be performed on the post-treated coatings.

In the following, a qualitative evaluation of fracture toughness for both the as-sprayed and HIPed coatings is presented. Figure 8 shows light microscope micrographs of the indentations performed on both coatings. The micrograph of the as-sprayed coating reveals an indentation taken at 10 kg load, which is surrounded by cracks. Measuring at the same conditions, it can be observed from the micrograph of the HIPed coatings (Fig. 8b) that there are no cracks surrounding the indentation. As this trend was consistent, it was concluded that the

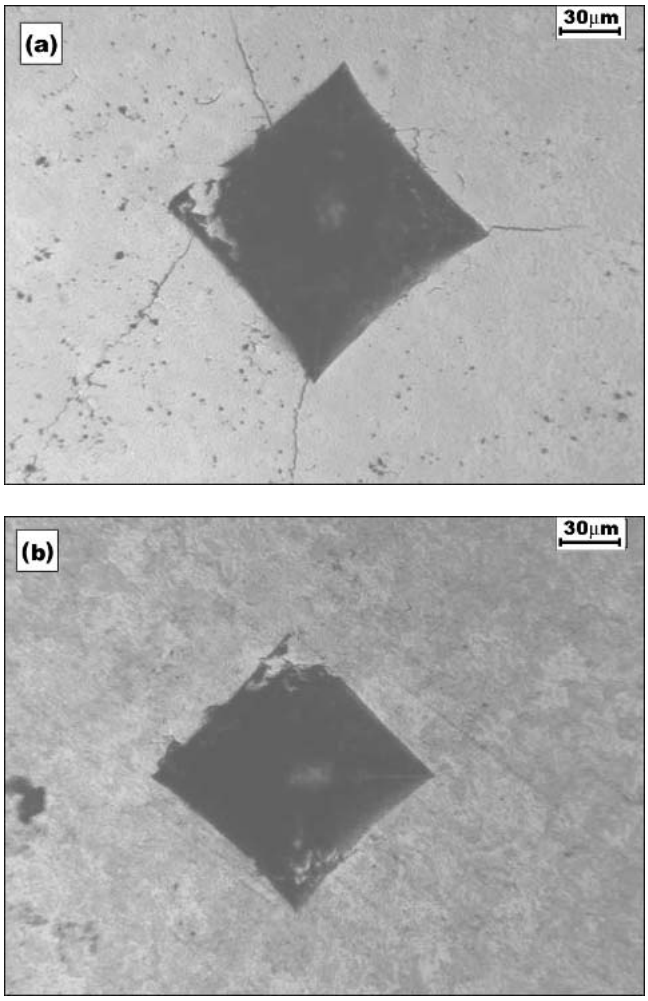

Fig. 8 Fracture toughness indentation on **(a)** as-sprayed, **(b)** HIPed coating (10 kg load)

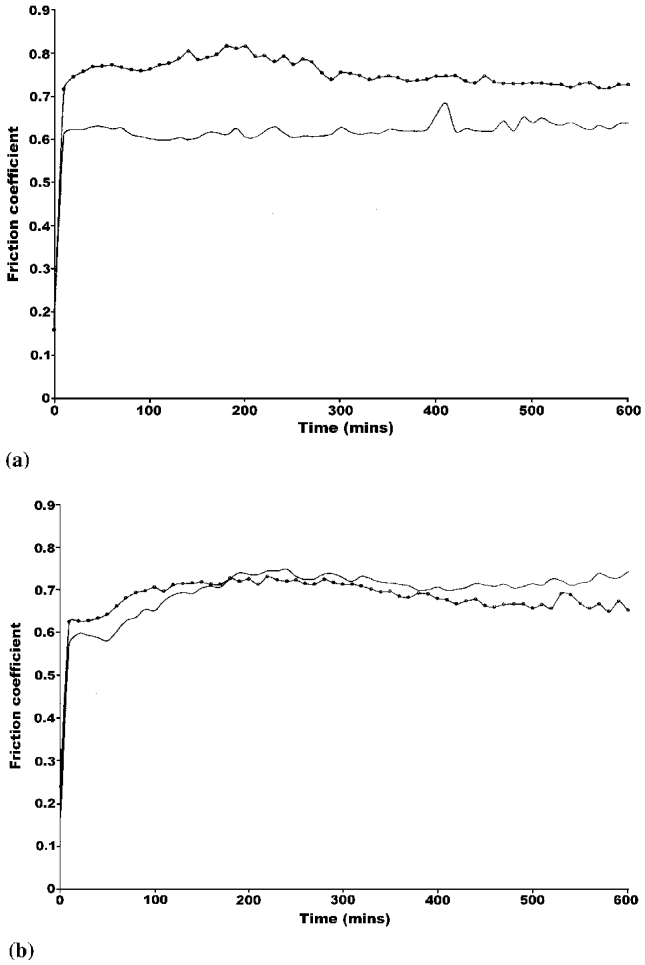

Fig. 9 Friction coefficients of (—•—) as-sprayed and (—) HIPed coatings tested versus **(a)** 400C steel and **(b)** Si_3N_4 ceramic (load 4 kg)

HIPing post treatment produced coatings that were relatively tougher than the initial as-sprayed ones. In fact, recalling also the results of microhardness measurements, it can be concluded that the post-treated coatings were harder and tougher than the untreated coatings. Typically one may expect that the increase in microhardness is accompanied by a decrease in fracture toughness of the material being studied. However, the results of this study show the contrary, suggesting that another process take place, which alter the above-mentioned interdependence between the hardness and fracture toughness. The authors believe that HIPing process produces an increase in bonding at the interface between the lamellae and thus an increase in toughness. The results of the elastic modulus confirm this hypothesis, as indicated in the next section.

3.2.3 Young's Modulus Measurements. Although the measurement of Young's modulus in thermal spray coatings is dependent upon the method as well as the direction of measurement, the universal harness method, which employs the force indentation curve during the hardness test, was particularly suited to the small size specimens to evaluate the relative changes in localised elastic modulus. On the surface of the as-sprayed coatings, the elastic modulus has an average value of 231 GPa, which increased to 247 GPa after HIPing post-treatment. The modulus measurements carried out on the coating cross section indicated far better improvement (of approximately 55%) in the elastic modulus, with as-sprayed and HIPed coating modulus of 190 and 330 GPa, respectively.

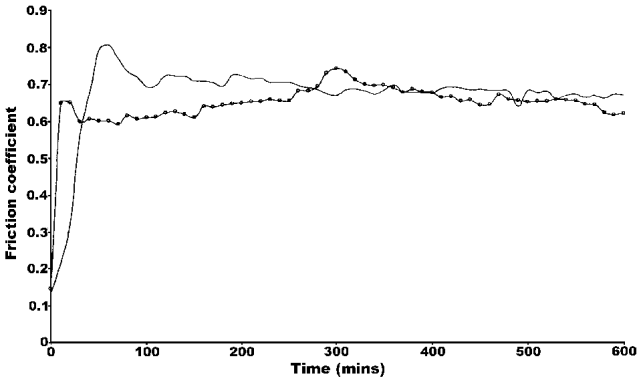

(a)

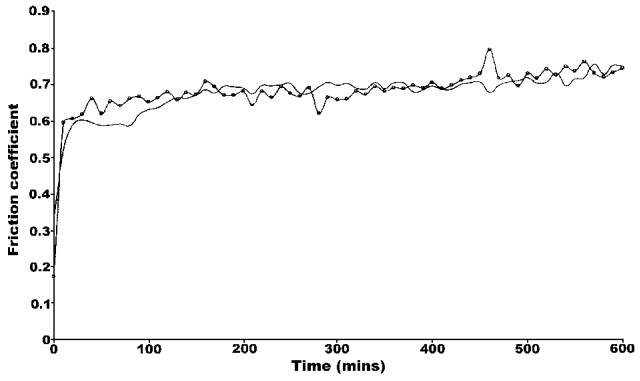

(b)

Fig. 10 Friction coefficients of (—•—) as-sprayed and (—) HIPed coatings tested versus **(a)** 440C steel and **(b)** Si_3N_4 ceramic (Load 6 kg)

3.3 Tribological Testing

3.3.1 Friction Behavior. The friction behavior of tested couples is shown in Fig. 9 and 10. All coatings show stable friction behavior without any significant increase in the friction coefficient during the tests. As expected, all tests start with a running-in stage, which last about 10-20 min, followed by a stabilization stage at a friction coefficient (μ) of around 0.6-0.7, which last all the remaining test time. As the testing conditions become more severe, e.g., coatings tested against ceramic balls under a load of 6 kg, some scatter of coefficient of friction can be noticed for both the as-sprayed and HIPed coatings. It is felt that this scattering is more likely brought about by the instability of the system at the test conditions used, e.g., particle pullout or debris entrapped in the contact area. The difference in the friction coefficient between the as-sprayed and HIPed coatings (around 0.1) can be observed only when the coatings slid over the steel balls under low load. The rest of the tests produced insignificant difference in friction between the tested couples.

3.3.2 Sliding Wear. Figure 11 exhibits the three dimensional interferometric plot of the section of coating wear scar which rubbed on steel balls. These coatings have wear scars, which are wider and shallower than those produced by ceramic

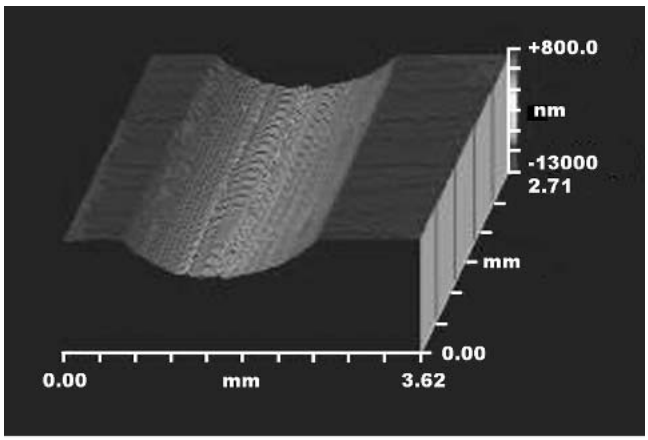

(a)

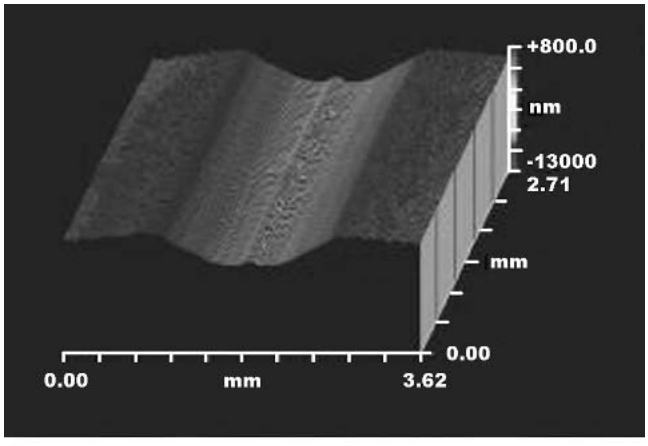

(b)

Fig. 11 Wear scars of **(a)** as-sprayed and **(b)** HIPed coatings worn versus 440C steel (load 4 kg)

balls (Fig. 12). In the former case, regardless of the type of coating, the width of the wear scars is about 2.5 mm, while in the latter case the width of the wear scars is around 1.9 mm. In general, as the depth of the wear scar decreased, its width increased, indicating more wear of the ball surface. The wear scar depth of the coatings, which rubbed against steel was approximately half of that in the coating-ceramic couples. These results indicate that the difference in the dimensions of the wear scars can be attributed to the hardness of the balls. As shown in Fig. 11, the wear scars of coatings, which rubbed against steel balls, were rough, suggesting that abrasion was one of the processes of material removal. On the other hand, the set of coatings tested against ceramic balls exhibit smooth wear scars with only few signs of abrasive marks (Fig. 12).

Figure 13 shows the wear volume data for various test configurations and provides a summary of wear results, both in terms of coating and ball material loss, as well as the total material loss for various test couples. It can be seen from Fig. 13 that for all couples, the coating material loss increased with increasing load. The post-treated coatings, independent of the balls, which slid against them, wear less for all test couples. This can be further appreciated from the interferometric images (Fig.

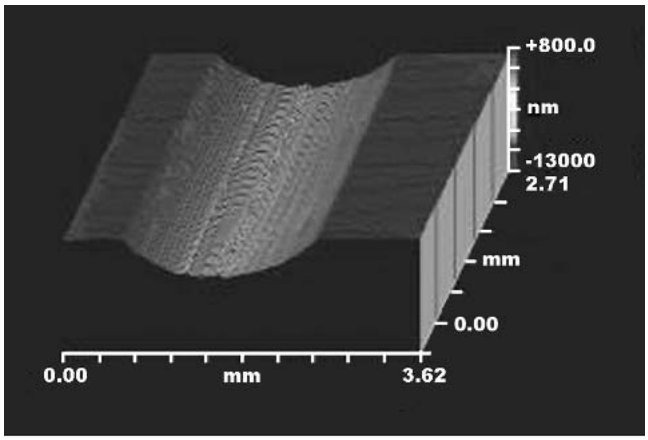

(a)

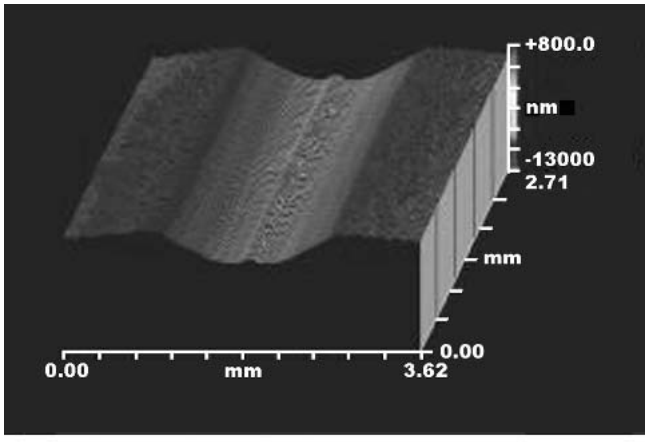

(b)

Fig. 12 Wear scars of **(a)** as-sprayed and **(b)** HIPed coatings worn versus Si_3N_4 (load 4 kg)

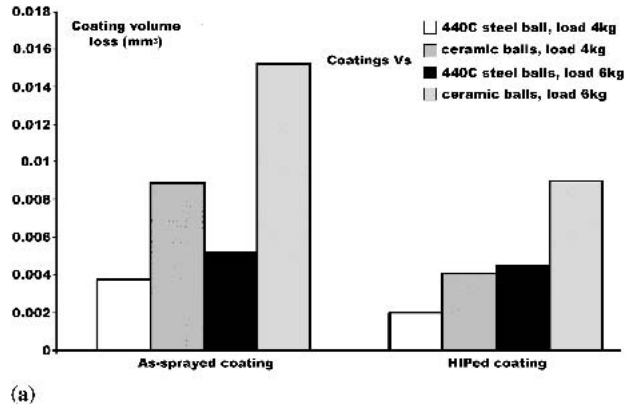

(a)

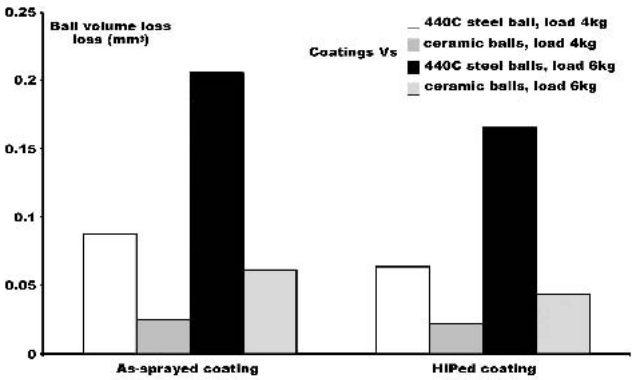

(b)

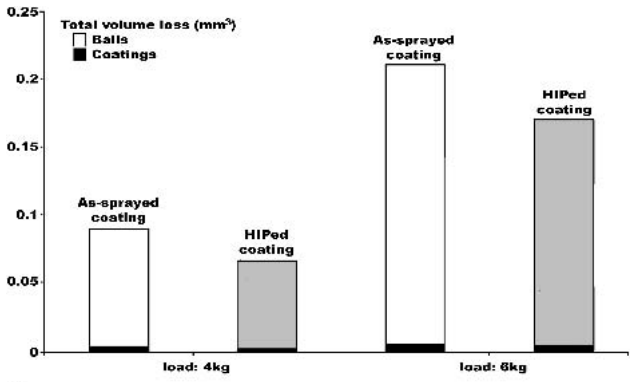

(c)

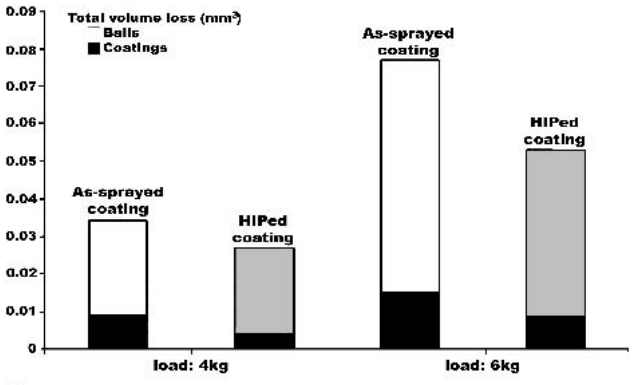

(d)

Fig. 13 Material loss (mm^3) of **(a)** coatings, **(b)** balls and total volume loss of coatings versus **(c)** steel, **(d)** Si_3N_4 balls

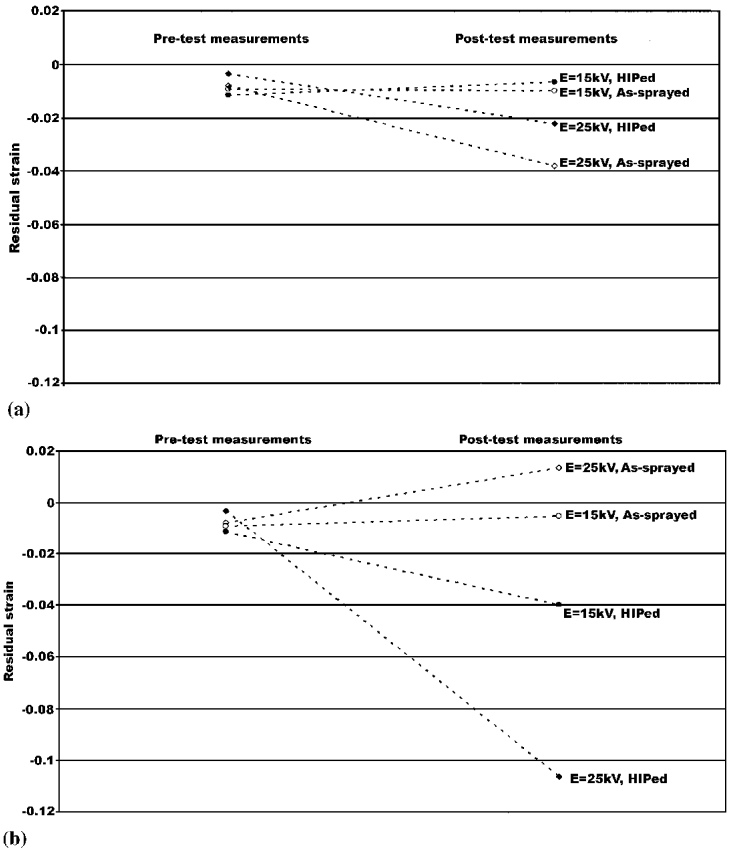

Fig. 14 Residual strain and stress pre and post wear tests (load 4 kg) on as-sprayed and HIPed coatings versus **(a, c)** steel and **(b, d)** ceramic

11 and 12), which clearly show smaller depth and width of wear scars for the HIPed coatings. The volume of HIPed material lost during all tests was almost half of that of as-sprayed coatings (Fig. 13a), except for the case of the coating which slid versus steel ball at 6 kg load, in which case the difference was not very significant. Figure 13(b) shows that the balls, which slid against the as-sprayed coatings, lose more material and, as mentioned before, the material loss of the ceramic balls is significantly lower than that of the steel ball. Hence, the volume loss of ball was superimposed on the lost coating material for each tested couple, to determine the effect of HIPing on the entire coating-ball system. Figure 13(c) and 13(d) show the result of such analysis and indicate that under the test conditions used, the systems which involved HIPed coatings have a better wear resistance. This behavior was consistent at two different loads and also with two different couples, indicating a general trend of improved sliding wear performance over a range of tribological conditions.

3.4 Residual Stress

Measurements of residual stress were carried out on all coatings before and after the sliding wear tests using synchrotron XRD. Residual stress and strain values were determined using $\sin^2\psi$ technique for three ψ angles at 15 and 25 keV. Although these energies are high, the 2θ angles were low and thus it was estimated that such power resulted in an approximate penetration depth of 5 μm. This measurement depth was particularly suited to evaluate the residual stress changes in pre and post tribo-tested coatings, where near surface changes dominate the wear process.

The stress on the surface was calculated from the following expression:

$$\sigma = \frac{E}{1+\nu}\frac{\partial(\varepsilon)}{\partial(\sin^2\psi)} = -\frac{E\cot\theta_d}{2(1+\nu)}\frac{\partial(\theta)}{\partial(\sin^2\psi)} \quad \text{(Eq 3)}$$

From which, we obtain:

$$\sigma = K\frac{\partial(\theta)}{\partial(\sin^2\psi)} \quad \text{(Eq 4)}$$

where E and ν are the Young modulus and Poisson's ratio, respectively; ε is the residual strain, θ is the diffraction angle, θ_d is the diffraction angle in a stress free condition, and ψ is the angle between the sample normal and diffraction-plane normal. The first term of Eq 4 is the x-ray elastic constant (K) and was measured using a conventional in situ four-point bending test equipment subjected to a known load within the elastic range. The measured value of the K was −1525 MPa. The last term of the equation is the slope of the best-fitted straight line of the 2θ-$\sin^2\psi$ plot.

To avoid using the experimentally determined x-ray elastic

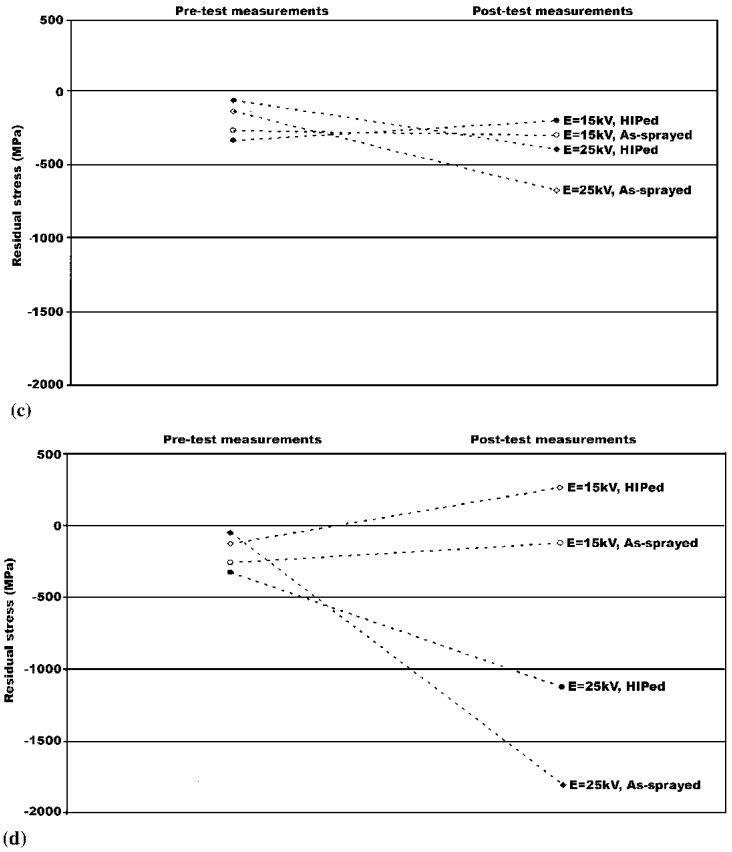

Fig. 14 cont. Residual strain and stress pre and post wear tests (load 4 kg) on as-sprayed and HIPed coatings versus **(a, c)** steel and **(b, d)** ceramic

constant, another approach based however on the same $\sin^2\psi$ technique was used to determine the residual strain. Thus, differentiating the relation:

$$\sigma = \frac{(d_\psi - d)E}{d(1+\nu)\sin^2\psi} \quad \text{(Eq 5)}$$

can be obtained:

$$\frac{\partial(d_\psi)}{\partial(\sin^2\psi)} = \frac{1+\nu}{E}\, d\sigma = m \quad \text{(Eq 6)}$$

which gives the residual strain as the ratio m/d. This ratio was calculated from the $d_\psi - \sin^2\psi$, where m is the slope and d is the intercept of the best fitted straight line. In Eq 5 and 6 the new terms are d_ψ, interatomic spacing from crystal planes in which the normal is defined by the angle ψ; d, interatomic spacing for crystal planes parallel to the specimen surface.

Figure 14 shows the residual stress and strain results of coatings in pre- and post-tribological test conditions for various couples, which were slid at a load of 4kg. Figure 14(a) and 14(c) indicate that the magnitude of residual stress and strain were dependent on the radiation energy and therefore on the penetration depth of the x-ray beam. At 15 keV energy, the magnitude of the compressive residual stress attenuates, suggesting that microcracking in the vicinity of the coating surface occurred during sliding wear tests, leading to compressive stress relaxation. At the energy of 25 keV, or in other words increasing the penetration depth, the compressive residual stress of the coatings changes, having a slightly higher value at the end of the wear test. However, as can be noticed from Fig. 14(c), the difference in the residual stress of all coatings in pre and post-tribological test conditions is relatively small.

As the ceramic ball replaces the steel ball and therefore the coating wear becomes more severe, the variation of the residual stress of pre and post measurements increases (Fig. 14b, d). The values of the compressive residual stress of the as-sprayed coatings measured before the wear tests are confined in an interval of about −270 MPa with a maximum at −332 MPa. The measurements performed on the wear track of the as-sprayed coatings showed a relaxation of the compressive residual stress. This change in residual stress was produced due to the fact that, under load, the as-sprayed coatings tend to develop cracks (Fig. 15), which propagate along and across the coatings. These cracks induce tensile residual stress (or an attenuation of compressive stress) in the coatings, and therefore the resulted residual stress system is either tensile or low compressive.

Contrary to that described above, in the case of worn HIPed coatings, at both penetration depths (15 and 25 keV) the magnitude of the compressive residual stress and strain increases. This was mainly due to the influence of material shakedown[30] during repeated sliding. Thus, when hard ceramic ball slid on the softer coating material, the load, which causes plastic deforma-

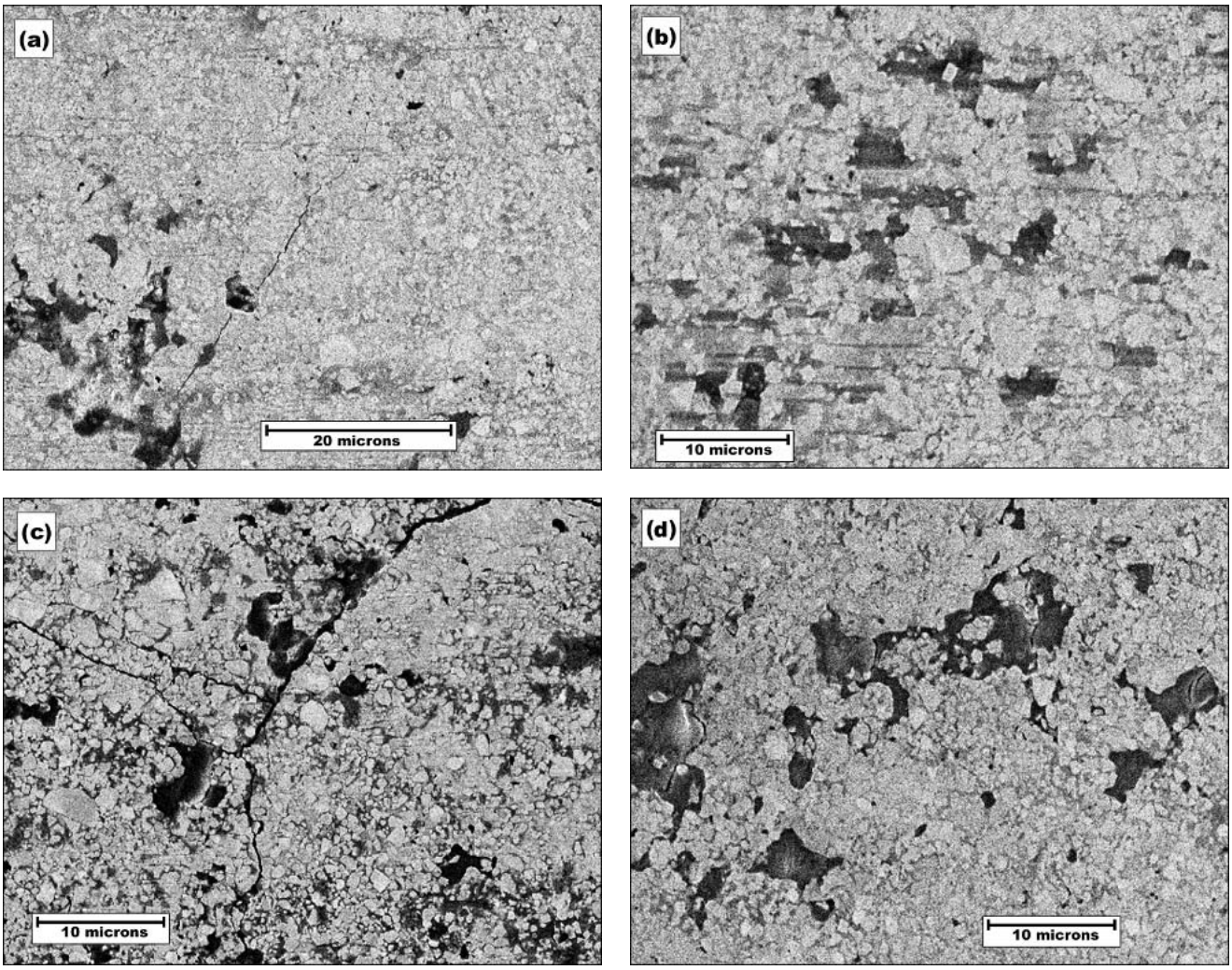

Fig. 15 SEM micrographs of **(a, c)** as-sprayed and **(b, d)** HIPed coating wear scars produced in contact with (a, b) steel balls, (c, d) Si_3N_4 balls (applied load: 4 kg)

tion in the early stages of testing, is accommodated elastically in the later stages of the test. This is possible due to the residual stresses, which develops in the coating surface vicinity and, in combination with contact stresses form a system of protective stresses. Further details of the mechanism of material shakedown due to contact loading in the near surface region can be found from Wong et al.[30]

4. Discussion

It is generally known that the high wear resistance of WC-Co thermal spray coatings is produced due to its high hardness and fracture toughness. Therefore, a coating subjected to any process that increases the hardness, and if possible, keeps the fracture toughness at acceptable levels will lead to improved wear resistance of coatings. It was seen in the current study that subjecting the thermal spray coatings to HIPing process leads to improved hardness and fracture toughness. This concomitant increase in hardness and fracture toughness is brought about by an improvement of the bonding at particle/binder interfaces. All these changes of the coating properties are related to the modifications that take place in the coating microstructure and also in the phase composition during the HIPing process.

It was seen that the deposition of coatings produces a certain degree of chemical reactions leading to secondary phases, complex η phases and amorphous phases. The published literature on the post-treatment of thermal spray coatings indicates that the recrystallization temperature of these amorphous phases is around 860 °C.[23,24] At the HIPing temperature of 850 °C used in this investigation, the recrystallization reactions took place, producing significant changes in the phase composition of the as-sprayed coatings. The recrystallized cobalt reacts with secondary phases and tungsten, producing η phases and additional amount of mono-tungsten carbide. These transformations alter both the hardness and the fracture toughness of the HIPed coatings.

Thus, although on one hand the hardness might be decreased by the elimination of secondary phase, the formation of complex η phases, which replaces the binder in the as-sprayed coating and the increased amounts of mono tungsten carbide, produced harder coatings. In terms of fracture toughness, the absence of secondary phase W_2C and tungsten W from the HIPed coatings,

which was reported to be the preferred crack propagation path, explains the crack-free indentations of the post-treated coatings (Fig. 8b). Regarding the structure of the coatings it was observed that the formation of prismatic shaped grains, which are rather close, packed produced homogeneous islands of tungsten carbide grains, agglomerates which, it is believed, increases the hardness of the coatings.

The ascending trend of the coating elastic modulus from the as-sprayed to HIPed coatings suggests that changes at the interface between lamellas takes place. Thus, metallurgical bonding between the lamellas across and along the coatings is thought to enhance the mechanical properties of the HIPed coatings.

4.1 Wear Mechanism

The high-magnification SEM micrographs of the as-sprayed coatings, which were tested against the steel ball and shown in Fig. 15(a), exhibit cracks, which propagated along and across the coating wear track. This distribution of cracks suggested that one of the wear mechanisms of as-sprayed coating/steel ball couple is micro and macro cracking. It was also observed that under the applied load, the cracks propagated even through the carbide grains leading to the spallation of the grains. Furthermore, signs of ploughing were observed on the entire length of the coating wear track and accordingly on the balls (Fig. 16a). Hence microcracking and abrasive wear mechanisms mainly contributed to the removal of coatings material. EDX analysis of the coating and ball wear scars after the sliding wear tests (Fig. 17) further confirm that during the wearing process, the material from the balls adheres to the coatings, and also the tungsten carbide grains can become embedded in the softer ball material. However, it is believed that the adhesive wear is a secondary wear mechanism during the sliding test, in which the material is alternatively transferred and removed.

For the as-sprayed coating/ceramic ball test couples, the micro-cracking and abrasive wear remain the main wear mechanism. However, the extent of material, which is removed in this test, is obviously higher than in the as-sprayed coating/steel ball

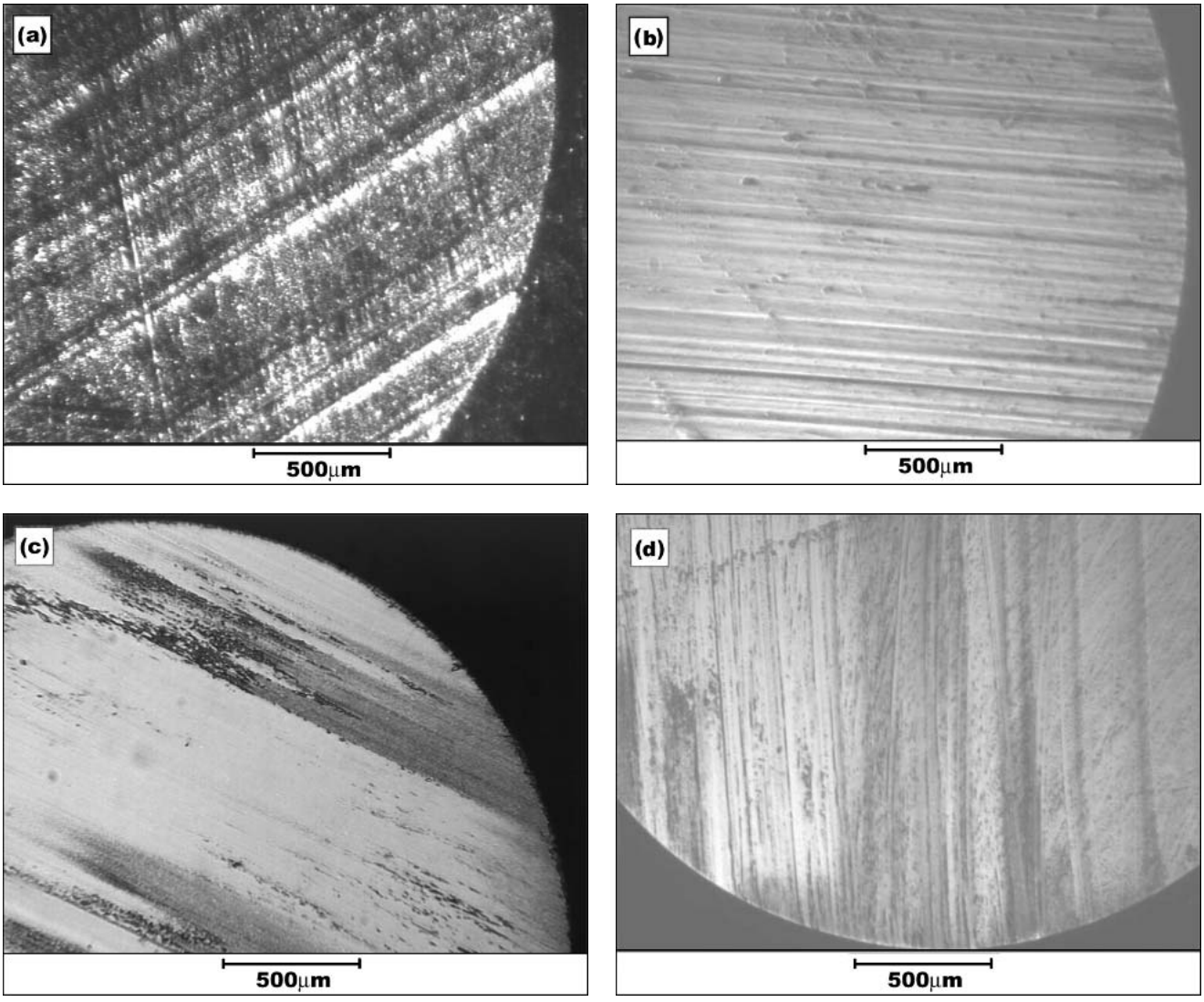

Fig. 16 Ball wear scars produced sliding **(a, c)** as-sprayed and **(b, d)** HIPed coatings versus (a, b) steel balls, (c, d) Si_3N_4 balls (applied load: 6 kg)

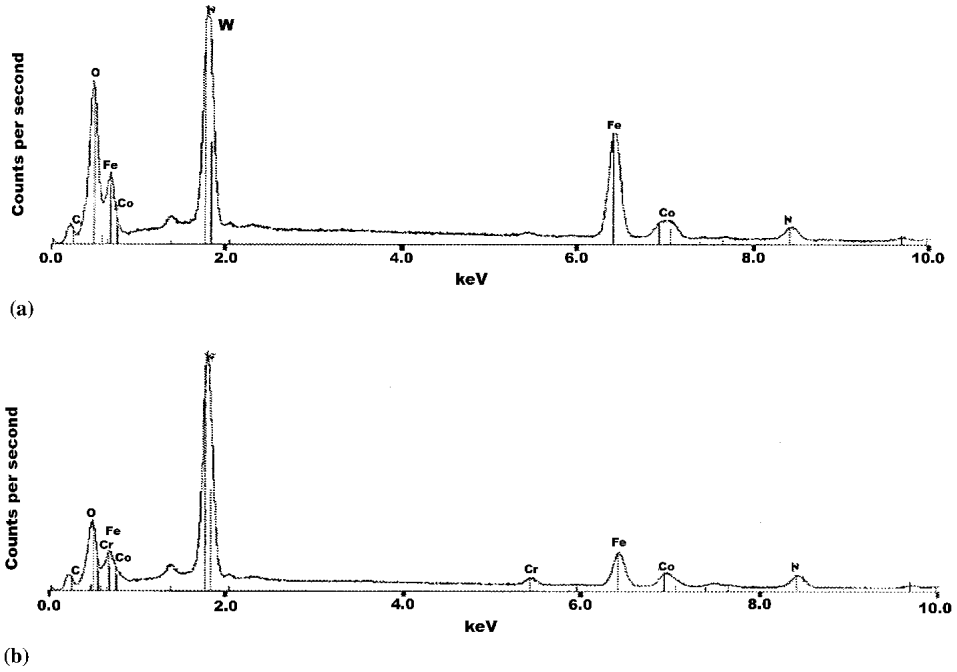

Fig. 17 EDX analysis on **(a)** as-sprayed and **(b)** HIPed coating wear scars produced in tests versus steel balls (applied load: 4 kg)

couple. The hardness of the ceramic ball, which is higher than that of the binder and of the carbide grains, is responsible for the amount of material removed. EDX results collected on the coatings indicate no material transfer from the ball; at least not in the later stages (end) of the test. EDX examination of the ceramic ball was not performed at this stage, as sputtered coating on ceramic ball prior to SEM analysis is thought to influence the EDX results. Hence, no conclusive evidence of material transfer influencing the wear mechanisms could be observed for ceramic couples.

As mentioned earlier in this paper, balls that slid against the HIPed coatings had less material loss. This behavior was consistent both for the steel and ceramic balls. The improved mechanical properties (modulus, hardness, toughness) of the HIPed coatings also altered the wear mechanisms. Thus, the indentation fracture toughness results which, despite the fact that they are qualitative, and lead to the conclusion that the relative toughness was improved, can be further confirmed by the morphology of the wear scars. Under the used applied load, no cracks were noticed on the wear tracks of HIPed coatings (Fig. 15). Therefore micro-cracking was excluded as a possible wear mechanism in all tests, which involved HIPed coatings.

In the HIPed coatings, the process of material removal starts with the extrusion of the binder material due to the higher hardness of the ball material with respect to the binder hardness. As a consequence, in the first stage, the carbide grains protrude from the coating, removing material from the ball in case of softer ball material, i.e., steel ball. This material becomes debris, which is either removed from the contact area or, as detected by EDX (Fig. 17), adheres on the coating wear scar. The EDX analysis being rather a qualitative than a quantitative analysis does not allow for an estimation of the material, which adhered on the coating. Therefore it was not possible to have a quantitative comparison between the removed material in the couples, which involved, on one hand, as-sprayed coatings and, on the other hand, HIPed coating. When the ceramic ball slid against the HIPed coating, coating spallation followed by the removal of carbide grains might also occur at this stage. Furthermore, as the wear process proceeds, the removal of the binder material continues. In the second stage, the carbide grains become unprotected by the loss of the binder material and are removed from the coating surface. They form the debris, which is either removed from the contact area or contribute to further material removal through three-body abrasion.

The last wear mechanism whose effects were seen preferable in the middle of the coating worn areas is plastic deformation, indicating improved material toughness. This is consistent with the increase in compressive residual stress and strain (Fig. 14) for HIPed post-tribo-test coatings and is indicative of material shakedown in the near surface region. Therefore it can be concluded that the properties of the HIPed coatings reduced the severity of the wear process. The microcracking of the coatings was eliminated while the level of abrasion, which was seen in the as-sprayed coating/balls couples, was reduced.

5. Conclusions

Hot isostatic pressing post treatment of thermal spray coatings was seen to improve the microstructure, physical properties, and, correspondingly the wear resistance of cermet coatings. As a result, the wear resistance of the post treated coatings was approximately twice that of the as-sprayed coatings. The counter bodies, either steel or ceramic ball, tested in contact with HIPed coatings also perform better in terms of the amount of material loss during the test.

Two main rationales for the improvement in physical properties and hence the improvement in sliding wear performance are

- Phase transformations: elimination of secondary phase W_2C and metallic tungsten W, alteration of amorphous binder phase through recrystallization of Co leading to precipitation of the η carbides
- Development of metallurgical bonding at the interface between the constituent lamellae of the coating, thereby increasing the coatings modulus after HIPing post treatment

The amount of material lost during the tribological testing was related to the differences in the wear mechanisms; i.e., as-sprayed coatings, which lost higher amounts of material, wear by microcracking, spallation, ploughing and material transfer. The wear mechanisms involved in the HIPed coating/ball test couples were extrusion of binder followed by the removal of the carbide grains, some levels of abrasion, plastic deformation and material transfer.

Acknowledgments

The authors would like to gratefully acknowledge the support of Dr. Michael Buchmann of Stuttgart University, Germany for elastic modulus measurements. Also the financial support of EPSRC, UK (Grant No. GR/R42584/01), CLRC-Daresbury Laboratory, UK (Grant No. FDA-38308), and Nuffield Foundation (Grant No. NAL/00294/G) is thankfully acknowledged.

References

1. A. Fritsch, R. Gadow, and A. Killinger: "Development of Highly Wear Resistant Coatings for Deflector Blades in Paper Industry" in *Thermal Spray: Surface Engineering via Applied Research* (Proceedings of ITSC 2000), C.C. Berndt, ed., ASM International, Materials Park, OH, 2000, pp. 1051-55
2. E. Strock, P. Ruggiero, and D. Reynolds: "The Effect of Off-Angle Spraying on the Structure and Properties of HVOF WC/CoCr Coatings" in *Thermal Spray 2001: New Surfaces for a New Millennium* (Proceedings of ITSC 2001), C.C. Berndt, K.A. Khor, and E.F. Lugscheider, ed., ASM International, Materials Park, OH, 2001, pp. 671-76
3. M.N. Nascimento, R.C. Souza, I.M. Miguel, W.L. Pigatin, and H.J.C. Voorwald: "Effects of Tungsten Carbide Thermal Spray Coating by HP/HVOF and Hard Chromium Electroplating on AISI 4340 High Strength Steel," *Surf. Coat. Technol.,* 2001, *138,* pp. 113-24.
4. J. Khedkar, A.S. Khanna, and K.M. Gupta: "Tribological Behavior of Plasma and Laser Coated Steels," *Wear,* 1997, *205,* pp. 220-27.
5. A. Chandak, R. Sivakumar, and G. Balasubramanian: "Tribological Solutions for Engineering Industries by HVOF—Topgun Spraying" in *Thermal Spray: Meeting the Challenges of the 21st Century, Proceedings of the 15th International Thermal Spray Conference,* C. Coddet, ed., ASM International, Materials Park, OH, 1998. pp. 531-53.
6. M.K. Keshavan and K.T. Kembalyan: "Wear Characterisation and Practical Applications of Thermal Spray Coatings in Drilling Applications" in *Proceedings of the 1993 National Thermal Spray Conference,* C.C. Berndt and S. Sampath, ed, ASM International, Materials Park, OH, 1993, pp. 635-41.
7. J.A. Peters and F. Ghasripoor: "Sliding Wear Behavior of Carbide Coatings" in *Advances in Thermal Spray Science and Technology: Proceedings of the 8th National Thermal Spray Conference,* C.C. Berndt and S. Sampath, ed., ASM International, Materials Park, OH, 1995, pp. 387-92.
8. K. Jia, T.E. Fisher, and B. Gallois: "Microstructure, Hardness and Toughness of Nanostructured and Conventional WC-Co Composites," *Nanostruct. Mater.,* 1998, *10,* pp. 875-91.
9. T.C. Hanson, C.M. Hackett, and G.S. Settles: "Independent Control of HVOF Particle Velocity and Temperature," *J. Therm. Spray Technol.,* 2002, *11*(1), pp. 75-85.
10. H. Ito, R. Nakamura, R. Shiroyoma, and M. Sasaki: "Post-treatment of Plasma Sprayed WC-Co Coatings by Hot Isostatic Pressing" in *Thermal Spray Research and Applications, Proceedings of the 3rd National Thermal Spray Conference,* Thomas F. Bernecki, ed., ASM International, Materials Park, OH, 1990, pp. 233-38.
11. H. Kuribayashi, K. Suganuma, Y. Miyamoto, and M. Koizumi: "Effects of HIP Treatment on Plasma-Sprayed Ceramic Coating Onto Stainless Steel," *Am. Ceram. Soc. Bull.,* 1986, *65,* pp. 1306-10.
12. K.A. Khor and N.L. Loh: "Hot Isostatic Pressing of Plasma Sprayed Ceramic Coatings" in *Ceramics-Adding the Value: Proceedings of the Third Int. Thermal Spray Conference,* C.C. Berndt, ed., 1992, pp. 804-09.
13. K.A. Khor, Y. Murakoshi, M. Takahashi, and T. Sano: "Plasma Spraying of Titanium Aluminide Coatings: Process Parameters and Microstructure," *J. Mater. Proc. Technol.,* 1995, *48,* pp. 413-19.
14. K.A. Khor and Y.W. Gu: "Hot Isostatic Pressing of Plasma Sprayed Yttria-Stabilized Zirconia," *Mater. Lett.* 1998, *34,* pp. 263-68.
15. H.C. Chen, E. Pfender, and J. Heberlein: "Structural Changes in Plasma-Sprayed ZrO_2 Coatings After Hot Isostatic Pressing," *Thin Solid Films,* 1997, *293,* pp. 227-35.
16. M. Buchmann, M. Escribano, R. Gadow, G. Burkle, M. Mahlich, and H.J. Fecht: "On the Elastic Mechanical Properties of Thermally Sprayed Coatings," in *Thermal Spray: Surface Engineering via Applied Research,* C.C. Berndt, ed, ASM International, Materials Park, OH, 2002, pp. 598-605.
17. W.J. Jarosinski, M.F. Gruninger, and C.H. Londry: "Characterisation of Tungsten Carbide Cobalt Powders and HVOF Coatings" in *Proceedings of the 1993 National Thermal Spray Conference,* C.C. Berndt, ed, ASM International, Materials Park, OH, 1993, pp. 153-57.
18. T. Shmyreva and D. Wang: "Structure-Wear Resistance Relationship for JP-5000TM Cermet Coatings" in *Thermal Spray: Surface Engineering via Applied Research,* C.C. Berndt, ed, ASM International, Materials Park, OH, 2002, pp. 300-05.
19. A.C. Savarimuthu, H.F. Taber, J.R. Shadley, E.F. Rybicki, W.C. Cornell, W.A. Emery, D.A. Somerville, and J.D. Nuse: "Sliding Wear Behavior of Tungsten Carbide Thermal Spray Coatings for Replacement of Chromium Electroplate in Aircraft Applications," *J. Therm. Spray Technol.* 2001, *10*(3), pp. 502-10.
20. D.A. Stewart, P.H. Shipway, and D.G. McCartney: "Microstructural Evolution in Thermally Sprayed WC-Co Coatings: Comparison Between Nanocomposite and Conventional Starting Powders," *Acta Mater.* 2000, *48,* pp. 1593-604.
21. H.L. de Villiers Lovelock: "Powder/Processing/Structure Relationships in WC-Co Thermal Sprayed Coatings: A Review of the Published Literature," *J. Therm. Spray Technol,* 1998, *7*(3), pp. 357-73.
22. W.J. Lenling, M.F. Smith, and J.A. Henfling: "Beneficial Effects of Austempering Post-Treatment on Tungsten Carbide Based Wear Coatings" in *Thermal Spray Research and Applications, Proceedings of the 3rd National Thermal Spray Conference,* Thomas F. Bernecki, ed., ASM International, Materials Park, OH, 1990, pp. 227-32.
23. J. Nerz, B. Kushner, and A. Rotolico: "Microstructural Evaluation of Tungsten Carbide-Cobalt Coatings," *J. Therm. Spray Technol.,* 1992, *1*(2), pp. 147-52.
24. C.J. Li, A. Ohmori, and Y. Harada: "Formation of an Amorphous Phase in Thermally Sprayed WC-Co," *J. Therm. Spray Technol.* 1996 *5*(1), pp. 69-73.
25. C. Verdon, A. Karimi, and J-L. Martin: "A Study of High Velocity Oxy-Fuel Thermally Sprayed Tungsten Carbide Based Coatings. Part 1: Microstructure," *Mater. Sci. Eng.,* 1998, *A246,* pp. 11-24.
26. P. Ostojic and R. McPherson: "Indentation Toughness Testing of Plasma Sprayed Coatings," *Mater. Forum* 1987, *10*(4), pp. 247-55.
27. M.F. Smith, D.T. McGuffin, J.A. Henfling, and W.J. Lenling: "A Comparison of Techniques for the Metallographic Preparation of Thermal Sprayed Samples," *J. Therm. Spray Technol.,* 1993, *2*(3), pp. 287-94.
28. D.J. Nolan and M. Samandi: "Revealing True Porosity in WC-Co Thermal Spray Coatings," *J. Therm. Spray Technol.*, 1997, *6*(4), pp. 422-24.
29. S.D. Glancy: "How Metallographic Preparation Affects the Microstructure of WC/Co Thermal Spray Coatings" in *1994 NTSC Proceedings: Thermal Spray Industrial Applications,* ASM International, Materials Park, OH, 1994, pp. 771-76.
30. S.K. Wong, A. Kapoor, and J.A. Williams: "Shakedown Limits on Coated and Engineered Surfaces," *Wear,* 1997, *203-204,* pp. 162-70.